

IRC –10414: a bow-shock-producing red supergiant star^{*}

V. V. Gvaramadze,^{1,2†} K. M. Menten,³ A. Y. Kniazev,^{4,5,1} N. Langer,⁶
J. Mackey,⁶ A. Kraus,³ D. M.-A. Meyer⁶ and T. Kamiński³

¹*Sternberg Astronomical Institute, Lomonosov Moscow State University, Universitetskij Pr. 13, Moscow 119992, Russia*

²*Isaac Newton Institute of Chile, Moscow Branch, Universitetskij Pr. 13, Moscow 119992, Russia*

³*Max-Planck-Institut für Radioastronomie, Auf dem Hügel 69, 53121 Bonn, Germany*

⁴*South African Astronomical Observatory, PO Box 9, 7935 Observatory, Cape Town, South Africa*

⁵*Southern African Large Telescope Foundation, PO Box 9, 7935 Observatory, Cape Town, South Africa*

⁶*Argelander-Institut für Astronomie der Universität Bonn, Auf dem Hügel 71, 53121, Bonn, Germany*

Accepted 2013 October 8. Received 2013 September 25; in original form 2013 August 31

ABSTRACT

Most runaway OB stars, like the majority of massive stars residing in their parent clusters, go through the red supergiant (RSG) phase during their lifetimes. Nonetheless, although many dozens of massive runaways were found to be associated with bow shocks, only two RSG bow-shock-producing stars, Betelgeuse and μ Cep, are known to date. In this paper, we report the discovery of an arc-like nebula around the late M-type star IRC –10414 using the SuperCOSMOS H-alpha Survey. Our spectroscopic follow-up of IRC –10414 with the Southern African Large Telescope (SALT) showed that it is a M7 supergiant, which supports previous claims on the RSG nature of this star based on observations of its maser emission. This was reinforced by our new radio- and (sub)millimeter-wavelength molecular line observations made with the Atacama Pathfinder Experiment (APEX) 12 meter telescope and the Effelsberg 100 m radio telescope, respectively. The SALT spectrum of the nebula indicates that its emission is the result of shock excitation. This finding along with the arc-like shape of the nebula and an estimate of the space velocity of IRC –10414 ($\approx 70 \pm 20 \text{ km s}^{-1}$) imply the bow shock interpretation for the nebula. Thus, IRC –10414 represents the third case of a bow-shock-producing RSG and the first one with a bow shock visible at optical wavelengths. We discuss the smooth appearance of the bow shocks around IRC –10414 and Betelgeuse and propose that one of the necessary conditions for stability of bow shocks generated by RSGs is the ionization of the stellar wind. Possible ionization sources of the wind of IRC –10414 are proposed and discussed.

Key words: Stars: kinematics and dynamics – stars: massive – circumstellar matter – stars: individual: (IRC –10414, WR 114, Betelgeuse).

1 INTRODUCTION

Massive stars form in compact star clusters (Lada & Lada 2003) and then find themselves in the field due to three major processes: few-body dynamical encounters (Poveda, Ruiz & Allen 1967; Gies & Bolton 1986), binary-supernova explosions (Blaauw 1961; Stone 1991) and cluster dissolution (Tutukov 1978; Kroupa, Aarseth & Hurley 2001). Unlike the last process, the first two ones can produce stars with very high (from tens to hundreds km s^{-1}) space velocities (Leonard 1991; Portegies Zwart 2000; Gvaramadze 2009;

Gvaramadze, Gualandris & Portegies Zwart 2009). Some of these, so-called runaway (Blaauw 1961), stars move supersonically through the interstellar medium (ISM) and give rise to bow shocks ahead of them. The bow shocks have a characteristic arc-like shape and can be detected in the optical (Gull & Sofia 1979), infrared (van Buren & McCray 1988), radio (Benaglia et al. 2010), and X-ray (López-Santiago et al. 2012) wavebands.

Interestingly, the vast majority of bow-shock-producing stars are either on the main-sequence or are blue supergiants (BSGs), while there are no Wolf-Rayet (WR) stars associated with distinct bow shocks and only two known bow-shock-producing red supergiants (RSGs), Betelgeuse (Noriega-Crespo et al. 1997b) and μ Cep (Cox et al. 2012). Moreover, most of these bow shocks were discovered in the

^{*} Based on observation obtained with the South African Large Telescope (SALT), programme 2011-3-RSA_OTH-002.

[†] E-mail: vgvaram@mx.iki.rssi.ru

mid-infrared and there are only few unambiguous detections in optical (Gull & Sofia 1979; Hollis et al. 1992; Kaper et al. 1997; Gvaramadze & Bomans 2008; Gvaramadze et al. 2011b) and other wave-bands (Benaglia et al. 2010; López-Santiago et al. 2012). Detection of optical bow shocks and their follow-up spectroscopy can be used for constraining parameters of the stellar wind and the local interstellar environment (e.g. Kaper et al. 1997; Hollis et al. 1992), and for estimating the shock and thereby the stellar space velocities, which in turn might serve as a basis for confronting results of numerical modelling of stellar wind bow shocks with observations (Meyer et al., in preparation).

In this paper, we report the discovery of an optical arc-like nebula around the late M-type star IRC−10414 and propose a possible explanation for its origin. We review the existing data on IRC−10414 in Section 2 and present the arc-like nebula in Section 3. Spectroscopic observations of IRC−10414 and the nebula, and the results of these observations are described and discussed in Section 4. In Section 5 we present and discuss our observation of the maser emission from IRC−10414. IRC−10414 and its nebula are further discussed in Section 6. We summarize in Section 7.

2 IRC−10414: OBSERVATIONAL DATA

IRC−10414 (also known as IRAS 18204−1344, RAFGL 2139 and OH 17.55−0.13) is a late M-type star and a prominent source of OH (Kolena & Pataki 1977), H₂O (Kleinmann, Sargent & Dickinson 1978; Lada et al. 1981) and SiO maser emission (Ukita & Goldsmith 1984). Hansen & Blanco (1975) classified IRC−10414 as an M8 star using objective-prism spectroscopy. Lockwood (1985) derived for IRC−10414 a spectral type of M6.5 III from visual and near-infrared photometry, while Kwok, Volk & Bidelman (1997) inferred a type of M7 on the basis of the *InfraRed Astronomical Satellite (IRAS)* low-resolution spectrum.

Assuming that IRC−10414 is an asymptotic giant branch (AGB) star with a luminosity of $L = 10^4 L_{\odot}$, Jura & Kleinmann (1989) derived a distance to the star of $d = 0.7$ kpc. This distance estimate is often quoted in the literature. Jura & Kleinmann (1989) also derived the mass-loss rate of IRC−10414 of $\dot{M} \approx 4 \times 10^{-6} M_{\odot} \text{ yr}^{-1}$ using the prescription by Jura (1987), which is based on a scaling of the *IRAS* 60 μm flux density.

Ukita & Goldsmith (1984) were the first to suggest that IRC−10414 is a RSG. Their suggestion was based on the large width of a single SiO maser emission profile and large circular polarization and velocity width of the OH maser emission, which are more typical of RSG than AGB stars (e.g. Le Bertre & Nyman 1990; Verheyen, Messineo & Menten 2012; see also Section 5.2).

Ukita & Goldsmith (1984) also discussed a possible membership of IRC−10414 of the OB association Sct OB3, but rejected it because the kinematic distance to IRC−10414 of ≈ 4.5 kpc, derived from the local-standard of rest (LSR) velocity of the star of $v_{\text{LSR}} = 42 \text{ km s}^{-1}$ (cf. Engels 1979; Lada et al. 1981; see also Section 5.2), is significantly larger than the distance to Sct OB3 of ≈ 1.7 kpc (Humphreys 1978). Using the kinematic distance they re-estimated the luminosity of IRC−10414 to be $L \approx 4 \times$

Table 1. Details of IRC−10414.

Spectral type	M7 I
RA(J2000)	18 ^h 23 ^m 17 ^s .90
Dec.(J2000)	−13°42′47″.3
l, b	17°5509, −0°1262
V (mag)	≈ 12
J (mag)	2.845±0.290
H (mag)	1.403±0.284
K_s (mag)	0.713±0.336
v_{LSR} (km s ^{−1})	43 ± 2
v_{∞} (km s ^{−1})	21 ± 2
P (d)	768.16; 2726.43

$10^5 L_{\odot}$, thereby further supporting the RSG nature of this star.

The RSG interpretation of IRC−10414 has recently been reinforced by Maeda et al. (2008). Using five-epoch very long baseline interferometry (VLBI) observations of IRC−10414, these authors measured proper motions of knots of the H₂O maser emission and estimated the distance to the star to be $d \approx 2$ kpc. Correspondingly, the luminosity and the mass-loss rate of IRC−10414 given in Jura & Kleinmann (1989) were scaled up to much larger values of $L \approx 10^5 L_{\odot}$ and $\dot{M} \approx 3 \times 10^{-5} M_{\odot} \text{ yr}^{-1}$, respectively.

In the following, we adopt a distance to IRC−10414 of $d = 2$ kpc. This distance is much smaller than the kinematic one derived by Ukita & Goldsmith (1984). The discrepancy could be resolved if IRC−10414 is a runaway star, i.e. if it has a significant peculiar radial velocity in addition to the radial velocity purely determined by circular rotation of the Galaxy, which is a natural assumption given the location of this star in the field (cf. Gvaramadze et al. 2012). This would essentially prohibit any “kinematic” distance determination¹. The runaway status of IRC−10414 is supported by the detection of a bow shock around this star (see Sections 3 and 4.3 for details) and by an estimate of its space velocity (Section 6.1.2).

IRC−10414 is indicated in the International Variable Star Index (VSX) as a variable (Watson, Henden & Price 2006) with the median V -band magnitude of 11.96 and the period of variation and its amplitude of $P = 768.16$ d and $\Delta V = 1.32$ mag, respectively. These figures were derived by Pojmański & Maciejewski (2005) from the light curve of IRC−10414 obtained from the All-Sky Automated Survey (ASAS). The period and amplitude of pulsations were recently revised by Richards et al. (2012), who used the ASAS V -band light curve on a much longer time interval to derive $P \approx 2726.43$ d and $\Delta V = 1.19$ mag. These authors also provided probabilistic classification of IRC−10414 with probability of being a semi-regular pulsating variable, RSG or Mira of 0.3450, 0.2744 and 0.1280, respectively.

Using the peak separation of 1612 MHz masing OH lines, Blommaert, van Langevelde & Michiels (1994) and Sevenster et al. (2001) estimated the terminal velocity of the stellar wind of IRC−10414 to be $v_{\infty} \approx 15 - 16 \text{ km s}^{-1}$ (see also Section 5.2).

¹ See, e.g., the famous (factor of 2) case of the kinematic distance of the giant molecular cloud W3 vs. the spectro-photometric distance of the Per OB associations (Xu et al. 2006).

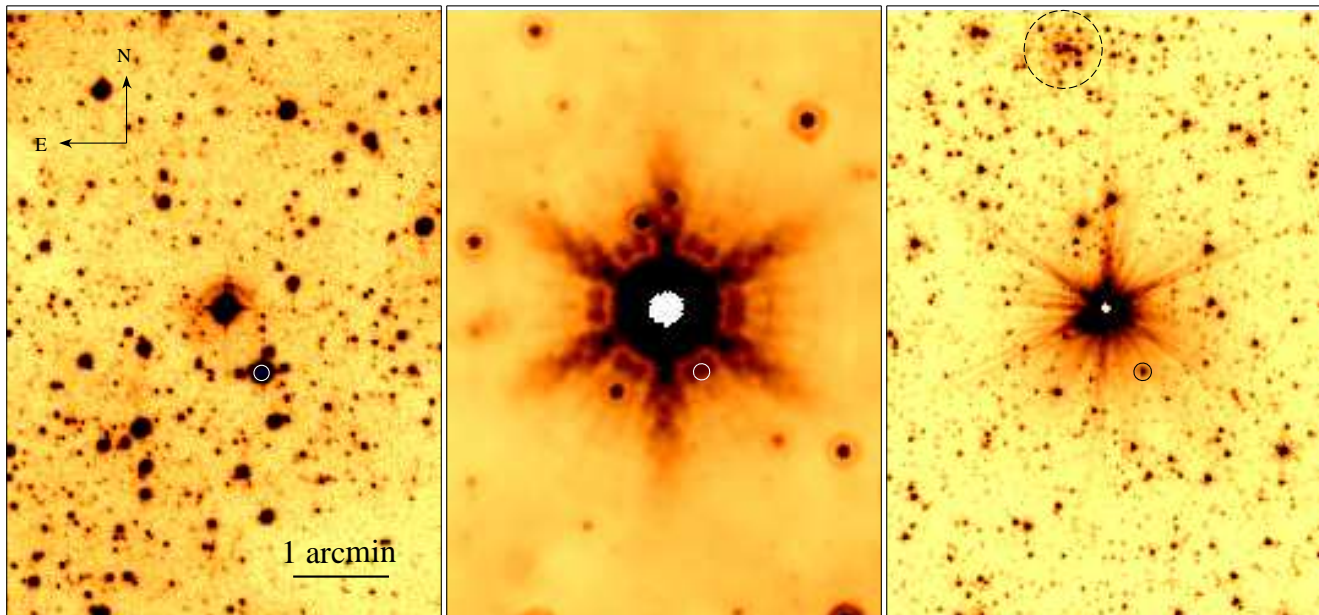


Figure 1. From left to right: SHS and *Spitzer* MIPS $24\ \mu\text{m}$ and IRAC $3.6\ \mu\text{m}$ images of the region around IRC-10414 and its associated arc-like nebula (both *Spitzer* images are highly saturated). The orientation and the scale of the images are the same. The position of the WC5 star WR 114 (located at ≈ 45 arcsec southwest of IRC-10414) is marked by a circle. A stellar concentration visible in the $3.6\ \mu\text{m}$ image at ≈ 2 arcmin to the north of IRC-10414 (marked by a dashed circle) is the background globular cluster Mercer 5. See text for details. At a distance of 2 kpc, 1 arcmin corresponds to ≈ 0.57 pc.

The details of IRC-10414 are summarized in Table 1. The spectral type is from Section 4.2. The coordinates and the J , H , K_s magnitudes are taken from the 2MASS (Two Micron All Sky Survey) All-Sky Catalog of Point Sources (Cutri et al. 2003). v_{LSR} and v_{∞} are from Section 5.2.

3 ARC-LIKE NEBULA AROUND IRC-10414

The arc-like nebula around IRC-10414 was serendipitously discovered during our search for bow shocks generated by OB stars running away from the young massive star cluster NGC 6611 (for motivation and the results of this search, see Gvaramadze & Bomans 2008). Using the SuperCOSMOS H-alpha Survey² (SHS; Parker et al. 2005), we searched for possible optical counterparts to bow shocks detected in the archival data of the Mid-Infrared Galactic Plane Survey (performed by the *Midcourse Space Experiment* satellite; Price et al. 2001) and found an arc-like structure (see the left panel of Fig. 1) at ≈ 1.1 degree (or ≈ 38 pc in projection) to the east of the cluster (see Section 6.1.2). We interpret this arc as a bow shock, as further discussed in Section 4.3. The orientation of the bow shock, however, is inconsistent with the possibility that its associated star was ejected from NGC 6611 (see Section 6.1.2). Using the SIMBAD data base³, we identified this star with the late M-type one IRC-10414. We found also that IRC-10414 is located at only ≈ 45 arcsec from the WC5 (Smith 1968) star WR 114

(see Fig. 1). A possible physical relationship between the two stars is discussed in Sections 6.1.2 and 6.2.2.

The stand-off distance of the bow shock, i.e. the minimum distance from the star at which the ram pressure of the stellar wind is balanced by the ram pressure of the ambient ISM, is $R_{\text{SO}} = \theta d$, where $\theta \approx 15$ arcsec is the angular separation between the apex of the bow shock and the star. At $d = 2$ kpc, $R_{\text{SO}} \approx 0.14$ pc; we neglected here a small geometrical factor (~ 1) taking into account inclination of the bow shock to the plane of the sky (see Section 6.1.2).

The bow shock interpretation of the arc implies that it should also be visible in the mid-infrared (e.g. van Buren & McCray 1988; Noriega-Crespo, van Buren & Dgani 1997a; Peri et al. 2012), while its relatively large angular extent suggests that it could be resolved with the Multiband Imaging Photometer for *Spitzer* (MIPS; Rieke et al. 2004) and the *Wide-field Infrared Survey Explorer* (*WISE*; Wright et al. 2010), which provide 24 and $22\ \mu\text{m}$ images at 6 and 12 arcsec resolution, respectively (cf. Gvaramadze, Kroupa & Pflamm-Altenburg 2010; Gvaramadze, Pflamm-Altenburg & Kroupa 2011a). Unfortunately, the very high infrared brightness of IRC-10414 made detection of an infrared counterpart to the arc impossible because of heavy saturation of the MIPS and *WISE* images. This is illustrated in the middle panel of Fig. 1, where we present the MIPS $24\ \mu\text{m}$ image of the star obtained within the framework of the 24 and 70 Micron Survey of the Inner Galactic Disk with MIPS (MIPSGAL; Carey et al. 2009).

IRC-10414 is also heavily saturated in all four (3.6 , 4.5 , 5.8 , and $8\ \mu\text{m}$) images obtained with the Infrared Array Camera (IRAC; Fazio et al. 2004) within the Galactic Legacy Infrared Mid-Plane Survey Extraordinaire (GLIMPSE; Benjamin et al. 2003). In the $3.6\ \mu\text{m}$ image we

² This survey provides narrow-band H α plus [N II] $\lambda\lambda 6548, 6584$ images of the Southern Galactic Plane and Magellanic Clouds with resolution of ~ 1 arcsec.

³ <http://simbad.u-strasbg.fr/simbad/>

found a stellar concentration at ≈ 2.8 arcmin to the north of IRC –10414 (see the right panel of Fig. 1), which turns out to be the background globular cluster Mercer 5 (Mercer et al. 2005; Longmore et al. 2011).

IRC –10414 was also covered by the Multi-Array Galactic Plane Imaging Survey (MAGPIS; Helfand et al. 2006) carried out with the Very Large Array (VLA), and by the *X-ray Multi-Mirror Mission (XMM-Newton)* observation of WR 114 (Oskinova et al. 2003). No radio or X-ray counterpart to the arc and the star were detected. On the other hand, we found that IRC –10414 is located at ≈ 1 arcmin to the northeast of the ~ 6 arcmin diameter (radio) shell of the supernova remnant (SNR) G017.4-00.1 (Brogan et al. 2006), which most probably is a background object (Pavlović et al. 2013).

4 SPECTROSCOPY OF IRC –10414 AND ITS ASSOCIATED ARC-LIKE NEBULA

4.1 Spectroscopic observations and data reduction

IRC –10414 and the arc-like nebula were observed within the framework of our ongoing programme of spectroscopic follow-up of bow-shock-producing stars (Gvaramadze et al. 2011b, 2013). The observation was conducted with the Southern African Large Telescope (SALT; Buckley, Swart & Meiring 2006; O’Donoghue et al. 2006) on 2012 April 20 with the Robert Stobie Spectrograph (RSS; Burgh et al. 2003; Kobulnicky et al. 2003). The long-slit spectroscopy mode of the RSS was used with a 1.25 arcsec slit width. The slit was oriented along the line connecting IRC –10414 and WR 114 (position angle ≈ 30 degrees; see Fig. 1). The grating GR900 was used to cover a total spectral range of $4200\text{--}9100$ Å with a final reciprocal dispersion of 0.97 Å pixel $^{-1}$ and FWHM spectral resolution of 4.74 ± 0.05 Å. The seeing during the observation was ≈ 1.5 arcsec. IRC –10414 was observed with two 600 s exposures for the blue ($4200\text{--}7250$ Å) part of the spectrum and one 60 s exposure for the red ($6420\text{--}9100$ Å) one. The spectrum of a Xe comparison arc was obtained to calibrate the wavelength scale as well as spectral flats to correct for pixel-to-pixel variations. A spectrophotometric standard star was observed after observation of the object for relative flux calibration. Primary reduction of the data was done with the SALT science pipeline (Crawford et al. 2010). After that, the bias and gain corrected and mosaicked long-slit data were reduced in the way described in Kniazev et al. (2008). The red end of the spectrum (> 8400 Å) shows significant fringing effects, which were corrected in the way described in Kniazev et al. (2013). The final, totally reduced and corrected for sensitivity, spectra of IRC –10414 and the arc-like nebula are shown in Figs. 2 and 3.

4.2 Spectral classification of IRC –10414

Fig. 2 shows that the spectrum of IRC –10414 is dominated by very strong molecular TiO absorption bands, which are typical of late M-type stars. The presence of the weak VO bands at $\lambda\lambda 5737, 6478, 7400, 7961$ and 7900 implies that IRC –10414 is an M7 star (Solf 1978; Turnshek et al. 1985), which agrees with the classification of this star based on the low-resolution *IRAS* spectrum (Kwok et al. 1997).

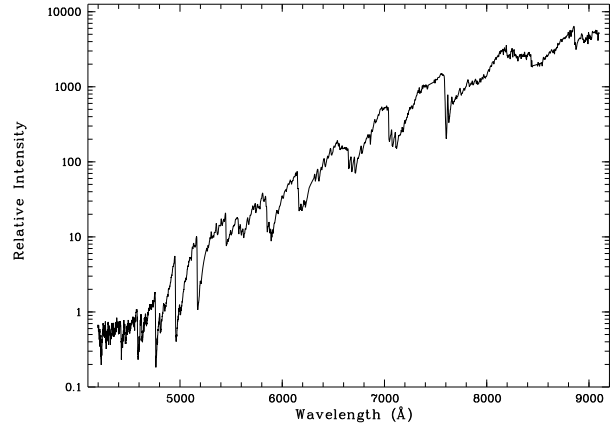


Figure 2. Observed spectrum of IRC –10414.

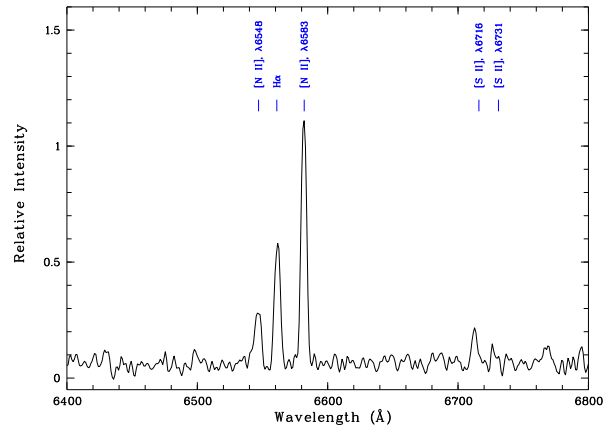


Figure 3. Observed spectrum of the arc-like nebula associated with IRC –10414 in the region of the $H\alpha$ line.

There are no solid criteria for assigning luminosity classes to late M stars because of paucity and variability of these stars. To determine the luminosity class for IRC –10414, we rely on the luminosity sensitive Ca II $\lambda\lambda 8498, 8542, 8662$ triplet, which is known to be a good luminosity indicator for early M stars (e.g. Jaschek & Jaschek 1987). It was found that the sum of EWs of lines of this triplet shows a good correlation with the stellar gravity, g , for stars with spectral type from F to M5 (Jones, Alloin & Jones 1984). Extrapolation of this correlation might be useful for constraining the luminosity classes of late M stars. Measurement of EWs of the Ca II triplet lines in the late M stars however is challenging because the TiO bands significantly affect their spectra, resulting in the depression of the continuum level and leading to the apparent reduction of EWs of the Ca II lines (e.g. Sharpless 1956; Zhu et al. 1999).

To measure EWs of the Ca II triplet, we follow the approach by Jones et al. (1984) and approximate the continuum between 8430 and 8852 Å as a straight line (cf. Beauchamp, Moffat & Drissen 1994). In doing so, we derived $EW(8498) \approx 5.5$ Å, $EW(8542) \approx 6.5$ Å and $EW(8662) \approx 5.5$ Å and estimated an uncertainty of ≈ 2 Å for these values. The total EW of the three Ca II lines of 17.5 ± 3.5 and fig. 3 in Jones et al. (1984) suggest that $\log g$ of IRC –10414 should

Table 2. Relative intensities and RVs of lines in the spectrum of the arc-like nebula associated with IRC-10414.

$\lambda(\text{\AA})$ Ion	$I(\lambda)/I(\text{H}\alpha)$	RV (km s ⁻¹)
6548 [N II]	0.53±0.05	-22.1±8.1
6563 H α	1.00±0.04	-1.4±2.9
6583 [N II]	1.89±0.04	-16.7±1.8
6716 [S II]	0.28±0.03	-10.9±9.9
6731 [S II]	0.12±0.03	-9.1±19.5

be negative (see also Section 6.1.1), which in turn implies the luminosity class of I for this star (cf. Beauchamp et al. 1994). Thus, IRC-10414 is an M7 I star.

4.3 Arc-like nebula as a bow shock

Fig. 3 presents the spectrum of the arc-like nebula in the same scale as the spectrum of IRC-10414 in Fig. 2. The comparison of the two spectra shows that in the region of the H α line the nebula is more than 6 mag fainter than the star. This, along with the proximity of the nebula to the star and the high extinction towards them (≈ 5 mag in the visual range; see Section 6.1.1), makes the spectroscopy of the former object a non-trivial observational task, which is impracticable with small telescopes. Even with the SALT we were not able to detect any emission lines in the blue spectrum of the arc. In the red part of the spectrum, we found the H α emission line and two forbidden emission doublets of [N II] $\lambda\lambda 6548, 6583$ and [S II] $\lambda\lambda 6716, 6731$, of which the nitrogen doublet is particularly strong (see Fig. 3). Relative intensities and heliocentric radial velocities (RVs) of these lines (measured by fitting Gaussians to them) are given in Table 2.

With so few detected lines in the spectrum of the arc-like nebula it is not possible to derive quantitative estimates of its elemental abundances, the electron temperature, T_e , or the extinction towards the arc. Still, some useful information can be extracted from the spectrum.

The ratio of the combined [S II] $\lambda\lambda 6716, 6731$ lines against H α can be used for distinguishing shock-heated nebulae (e.g. SNRs and Herbig-Haro objects) from photoionized ones [e.g. H II regions and most planetary nebulae (PNe)]. In SNRs this ratio is enhanced with respect to that measured for H II regions and typically is $\geq 0.3 - 0.4$ (e.g. Fesen, Blair & Kirshner 1985; Stupar & Parker 2009; Leonidaki, Boumis & Zezas 2013). For the arc-like nebula we found the [S II]/H α ratio of 0.4, which suggests that the ionization of the nebula is because of shock-heating.

The high intensity ratio of the [S II] doublet relative to H α is also observed in old, low-density PNe, which show signatures of interaction with the ISM (e.g., Sh 2-176: Sabadin, Minello & Bianchini 1977; Sh 2-216: Fesen, Blair & Gull 1981; Reynolds 1985; PFP 1: Pierce et al. 2004) and whose emission can also be attributed to shock-heating. The PN nature of the arc, however, can be rejected on the basis of the plot of the [S II] electron number density (as measured from the [S II] $\lambda\lambda 6716, 6731$ line intensity ratio; see below), n_e , versus the radius for PNe given in Phillips (1998; see fig. 5 therein). According to this plot, a PN with $n_e \lesssim 100 \text{ cm}^{-3}$ must have a radius of $\gtrsim 0.3$ pc. This would indicate a dis-

tance to IRC-10414 of $\gtrsim 4$ kpc and a luminosity of this star of $\gtrsim 6 \times 10^5 L_\odot$, which is too high for central stars of PNe. Since the arc around IRC-10414 is definitely not a SNR, nor a Herbig-Haro object, we conclude that it is a bow shock. The bow shock interpretation of the arc-like nebula is also supported by the runaway status of IRC-10414 (see Section 6.1.2), and by morphology of the nebula itself.

The [S II] $\lambda\lambda 6716, 6731$ line intensity ratio can be used to derive n_e in the line-emitting region (Krueger, Aller & Czyzak 1970; Saraph & Seaton 1970). Note that the measured ratio of 2.33 ± 0.63 significantly exceeds the theoretical one of ≈ 1.4 (Krueger et al. 1970) and the one based on the apparent peak intensities (see Fig. 3). This discrepancy is due to the weakness of the [S II] $\lambda 6731$ line, whose shape is strongly affected by the noise. Nevertheless, the measured and theoretical ratios are in agreement with each other at 1.4 sigma level, and both are in the low-density limit. Thus, we can only put an upper limit on n_e of $\leq 100 \text{ cm}^{-3}$.

The [N II] and [S II] line intensities can be used to estimate the nitrogen to sulphur abundance ratio, which is almost independent of n_e and T_e , provided that $n_e \leq 100 \text{ cm}^{-3}$ and $T_e \leq 10^4$ K. In this case, the abundance ratio is given by (see Benvenuti, D’Odorico & Peimbert 1973 and references therein):

$$\frac{N(\text{N}^+)}{N(\text{S}^+)} = 3.61 \frac{I(6584)}{I(6716 + 6731)}. \quad (1)$$

Unfortunately, the spectrum of the arc is not deep enough to detect the electron temperature diagnostic line [N II] $\lambda 5755$. Nonetheless, it is likely that T_e in the line-emitting region is $\leq 10^4$ K. Using equation (1) and Table 2, one finds $N(\text{N}^+)/N(\text{S}^+) \approx 17$, which more than three times exceeds the solar value of 5.12 (Asplund et al. 2009). This estimate suggests that the line-emitting material is enriched in nitrogen and that its composition might reflect that of the stellar wind (cf. Reimers et al. 2008), which in RSGs is enhanced in N by a factor of $\sim 3 - 5$ because of the dredge-up of the nuclear processed gas (e.g. Brott et al. 2011). We conclude therefore that the emission of the bow shock at least partially originates in the shocked stellar wind.

The overabundance of N could be responsible for the very high [N II]/H α ratio observed in the arc. Such high line ratios were also detected in circumstellar nebulae around some evolved massive stars, e.g. the WN8h star WR 124 (Esteban et al. 1991) and the luminous blue variable (LBV) star AG Car (Smith et al. 1997), which might be considered as the evidence that these stars have evolved through the red supergiant phase (e.g. Smith et al. 1997; but see Lamers et al. 2001 for a different explanation of enhanced N abundance in LBV nebulae). Similarly, the high [N II]/H α ratios observed in some SNRs, e.g. W50 (Kirshner & Chevalier 1980) and SNR G279.0+1.1 (Stupar & Parker 2009), might be due to supernova explosions within pre-existing wind-driven shells (created by supernova progenitor stars), which are enriched by the RSG wind material.

Note that the high [N II]/H α ratio might not be solely caused by the enhanced nitrogen abundance. It can also be inherent to spectra of photoionized nebulae of normal chemical composition, e.g., ionized regions surrounding the so-called supersoft X-ray sources (Rappaport et al. 1994) or ionization fronts (Henney et al. 2005). Note also that according to models presented in the two afore-cited papers, the

high-intensity nitrogen lines in the spectra of photoionized nebulae should be accompanied by very strong [O I] $\lambda 6300$ emission line (stronger than or comparable to the $H\alpha$ line). However, we did not detect this line in the spectrum of the nebula around IRC-10414, which implies that its intensity is less than 10 – 20 per cent of that of the $H\alpha$ line.

To summarize, the sum of evidence strongly supports the view that the arc around IRC-10414 is a bow shock.

5 MOLECULAR LINE EMISSION FROM IRC-10414

5.1 Millimeter-wavelength and radio observations

The millimeter-wavelength observations were made with the Atacama Pathfinder Experiment (APEX) 12 meter telescope (Güsten et al. 2006) under (for its Atacama desert site) moderate weather conditions. On 2012 April 4 and May 8 we used the APEX-1 receiver, which is part of the Swedish heterodyne facility instrumentation (Vassilev et al. 2008), to observe the SiO $J = 5 - 4$ rotational transition, both in the vibrational ground and the first excited state ($v = 0$ and 1); see Table 3 for information on the observed lines. The data were calibrated using the standard chopper wheel method. Employing the 2.5 GHz total bandwidth of the newest version of the APEX facility Fast Fourier Transform Spectrometer (FFTS; Klein et al. 2006) available at the time, each ($v = 0$ and 1) pair of lines could be observed in one band pass. The FFTS's 2.5 GHz were split into 32768 channels with a spacing of 76.3 KHz, which corresponds to 0.105 and 0.088 km s^{-1} at 217 and 260 GHz, respectively. For clarity reasons the spectra shown in Fig. 4 have been binned in $\approx 1.6 \text{ km s}^{-1}$ wide channels. On 2013 August 14, we used an upgraded version of the First Light APEX Submillimeter Heterodyne instrument (FLASH; Heyminck et al. 2006), which is an MPIFR principal investigator instrument, to observe the SiO $v = 0$ and 1 $J = 7 - 6$ lines around 302 GHz. Like APEX-1, FLASH is a two sideband (2SB) receiver. However, its bandwidth is a larger 4 GHz for each sideband. The wide bandwidth allowed serendipitous detection of two lines from sulfur monoxide (SO); see Table 3.

Conversion to flux density units (in Jy) and a main-beam brightness temperature scale (in K) was established by interpolating the aperture and main-beam efficiencies, η_A and η_{MB} , given by Vassilev et al. (2008) and Güsten et al. (2006). Values are $\eta_A = 0.67$ and $\eta_{MB} = 0.82$ for the SiO $J = 5 - 4$ lines, and $\eta_A = 0.60$ and $\eta_{MB} = 0.73$ for the $J = 7 - 6$ and the SO lines. The FWHM beam widths are 29 arcsec for the former pair of lines and 21 arcsec for the latter four.

The centimeter wavelength observations were made with the MPIFR Effelsberg 100 m radio telescope. The 22.2 GHz observations of the H_2O maser line (made on 2012 July 4) and the 1.7 GHz OH transitions (2012 June 10) used the facility K- and L-band receivers, respectively. For both sets of observations, the facility FFTS afforded two 100 MHz wide modules, each with 32768 frequency channels. One channel detected left, the other right circularly polarized radiation. For the OH lines, the channel spacing corresponds to 0.55 km s^{-1} in velocity units, for the H_2O

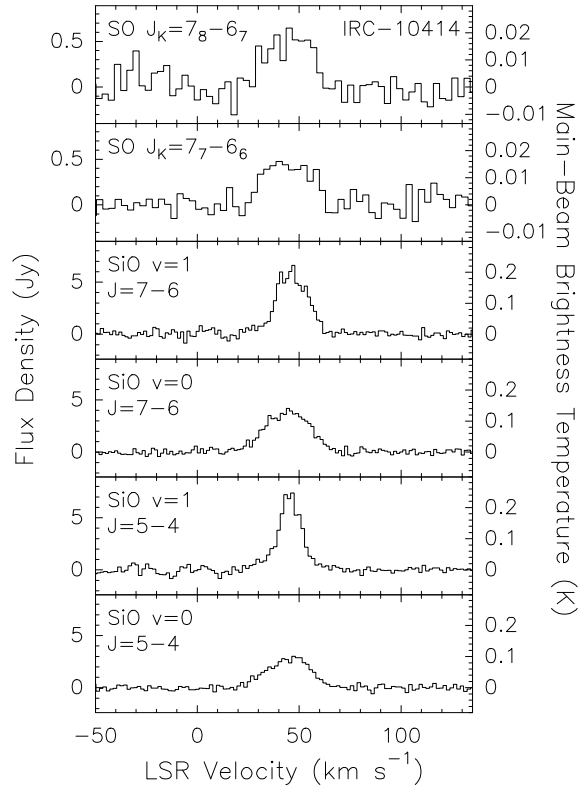


Figure 4. Sulfur monoxide (SO) and Silicon monoxide (SiO) lines observed toward IRC-10414 with APEX. Bottom to top, spectra of the $v = 0$ and 1, $J = 5 - 4$ and $v = 0$ and 1, $J = 7 - 6$ transition are plotted. The left and right abscissa show a flux density and a main-beam-brightness temperature scale, respectively. For clarity reasons, the SO lines were smoothed to a channel spacing of $\approx 3.0 \text{ km s}^{-1}$ and the SiO lines to $\approx 1.5 \text{ km s}^{-1}$.

line to 0.04 km s^{-1} . For Fig. 5 the spectrum of the latter was smoothed to 0.16 km s^{-1} . To calibrate the spectra, corrections for the atmospheric attenuation as well as for the gain-elevation effect were applied. Finally, the spectra were converted into flux density by applying the aperture efficiencies for both receivers (L-band: 0.53, K-band: 0.32). The aperture efficiencies were checked by observations of known flux density calibrators like 3C 286, 3C 48 and NGC 7027 (see Baars et al. 1977).

5.2 Molecular line results and discussion

The results of our spectral line observations are presented in Table 3. Fig. 4 shows the spectra of the SO $J_K = 7_7 - 6_6$ and $7_8 - 6_7$ and the SiO $J = 5 - 4$ and $J = 7 - 6$ transitions from within the $v = 0$ and the $v = 1$ states observed with the APEX telescope, while Fig. 5 presents the Effelsberg spectra of the 22.2 GHz H_2O maser lines, the 1612 MHz OH “satellite” hyperfine structure (hfs) line and the 1665 and 1665 MHz “main” hfs lines. For all the OH lines, both right and left circularly polarized (RCP and LCP) spectra are shown. The 1720 MHz satellite line was, as is expected for evolved stars, not detected. From the observed total velocity spread and its centroid, we determine for IRC-10414 $v_\infty = 21 \pm 2 \text{ km s}^{-1}$ and $v_{\text{LSR}} = 43 \pm 2 \text{ km s}^{-1}$ (which corresponds to a heliocentric radial velocity of $v_{r,\text{hel}} = 28.6 \pm 2.0 \text{ km s}^{-1}$).

Table 3. Results of molecular line observations.

Species	Transition	Frequency (MHz)	E_l (K)	Polarization	v -range (km s ⁻¹)	$\int S dv$ (Jy km s ⁻¹)
SiO	$v = 0, J = 5 - 4$	217104.98	20.8		[22,69]	72.1(1.1)
	$v = 1, J = 5 - 4$	215595.95	1790.0		[22,68]	104.6(1.7)
	$v = 0, J = 7 - 6$	303926.81	43.8		\approx [20,68]	103.0(1.2)
	$v = 1, J = 7 - 6$	301814.33	1812.8		\sim [21,61]	113.2(3.0)
SO	$J_K = 7_7 - 6_6$	301286.12	56.5		\sim [24,63]	12.8(1.4)
	$J_K = 7_8 - 6_7$	304077.84	47.6		\sim [28,62]	14.3(1.5)
H ₂ O	$6_{16} - 5_{23}$	22235.08	642.5	LCP+RCP	[29,58]	226(1)
OH	$F = 1 - 2$	1612.231	0.0	LCP	[23,62]	13.7(0.2)
				RCP	[25,63]	15.2(0.2)
	$F = 1 - 1$	1665.408	0.0	LCP	[23,63]	17.5(0.2)
				RCP	[26,62]	13.5(0.2)
	$F = 2 - 2$	1667.359	0.0	LCP	[20,61]	32.0(0.2)
				RCP	[22,62]	34.4(0.2)
	$F = 2 - 1$	1720.530	0.0	LCP	[20,63]	< 0.9
				RCP	[20,63]	< 0.9

Columns are: molecule, quantum number of transition, rest frequency, energy above ground state of lower energy level, (for OH:) sense of polarization, velocity range covered by line (FWZP) and integrated flux density. For the H₂O line the quantum numbers are $J_{K_a K_c}$. The OH lines are magnetic hfs transitions between sublevels of the $^2\Pi_{3/2}, J = 3/2$ rotational ground state. For them, flux densities in left and right circular polarization (LCP and RCP) are listed. For the non-detected OH 1720 MHz line the quoted flux density upper limit has been calculated from three times the rms noise value of the spectrum and assuming a line width equal to that of the detected OH transitions, i.e. [20,63] km s⁻¹.

Our value for v_{LSR} is consistent with that determined by Ukita & Goldsmith (1984) for the $v = 1, J = 2 - 1$ SiO maser line, while v_∞ is larger than the figure of 15 – 16 km s⁻¹ inferred by Blommaert et al. (1994) and Sevenster et al. (2001) from the separation of the red- and blue-shifted peaks of the OH 1612 MHz line. The reason for the difference may be that during the epochs at which these authors' data were taken maser features at velocities closer to v_{LSR} than v_∞ may have dominated the spectrum.

Notably, the intensity of the OH 1612 MHz line is between 1 and 2 Jy, which is similar to values found during previous observations (Blommaert et al. 1994; Sevenster et al. 2001). The H₂O maser's flux density exceeds 100 Jy, as during all its previous measurements (see Kleinman et al. 1978; Lada et al. 1981; Maeda et al. 2008).

To put these findings in a context, we first briefly summarize maser emission from evolved, oxygen-rich stars (see Habing 1996 for an extensive treatment). We start with SiO masers, which are formed within a few stellar radii from the photosphere where the high density and SiO abundance and an intense infrared radiation field fulfil the pumping requirements, which require densities between 10⁹ and 10¹⁰ cm⁻³ and temperatures > 1000 K (Lockett & Elitzur 1992; Bujarrabal 1994), and allow build up of sufficient maser gain. Further away from the star, SiO depletes into the forming dust grains although enough remains in the gas phase to produce thermally excited SiO emission arising from large parts of the circumstellar envelope and reaching terminal velocity. H₂O maser emission arises from a still relatively warm region outside of the dust formation region in which the outflow has reached much or most of v_∞ , roughly from the same region as main-line (1665 and 1667 MHz) OH masers. In contrast, the satellite (1612 MHz) OH masers arise from a much

larger region. The above picture, well illustrated by fig. 1 of Chapman & Cohen (1986) for the case of the RSG VX Sgr, is consistent with observations of the few known OH emitting RSGs (i.e., VX Sgr, VY CMa, NML Cyg) and so-called OH/IR stars, which are typically AGB stars of more than one solar mass with higher mass-loss rates than Mira variables and, consequently, optically opaque envelopes. Solar mass oxygen-rich AGB stars (“Miras”), which have lower mass-loss rates than RSGs, usually don't show 1612 MHz emission at all. All maser lines show significant variability. In particular, for Miras the narrow features in SiO maser spectra completely change from one stellar cycle (of ~ 300 d or less) to the next.

The maser phenomenology of IRC-10414 shows clear deviations from the canonical picture outlined above. SiO masers from both RSGs and Miras from the $v = 1$ or higher vibrational state typically show several narrow (from ~ 1 to a few km s⁻¹ wide) maser features that group around v_{LSR} within a velocity interval that is significantly smaller than $2v_\infty$. SiO lines from the vibrational ground state ($v = 0$) mostly have smooth, parabolic profiles, indicating spatially unresolved optically thick emission, in some cases (for the $v = 0, J = 1 - 0$ line) superposed with a few maser spikes. In the case of IRC-10414, both the $v = 0, J = 5 - 4$ and $7 - 6$ lines behave as expected, showing(almost) parabolic profiles, with a large full width at zero power (FWZP) of $\approx 2v_\infty$. Remarkably, the $v = 1$ lines have similar widths, but more asymmetric, smooth (not spiky) profiles that are more strongly skewed to higher velocity than those of the $v = 0$ lines. While the profile and intensity of the $v = 0$ lines are consistent with thermal emission with a small beam filling factor (given its 0.1 K main-beam brightness temperature), the $v = 1$ line *must definitely* be masing and arise

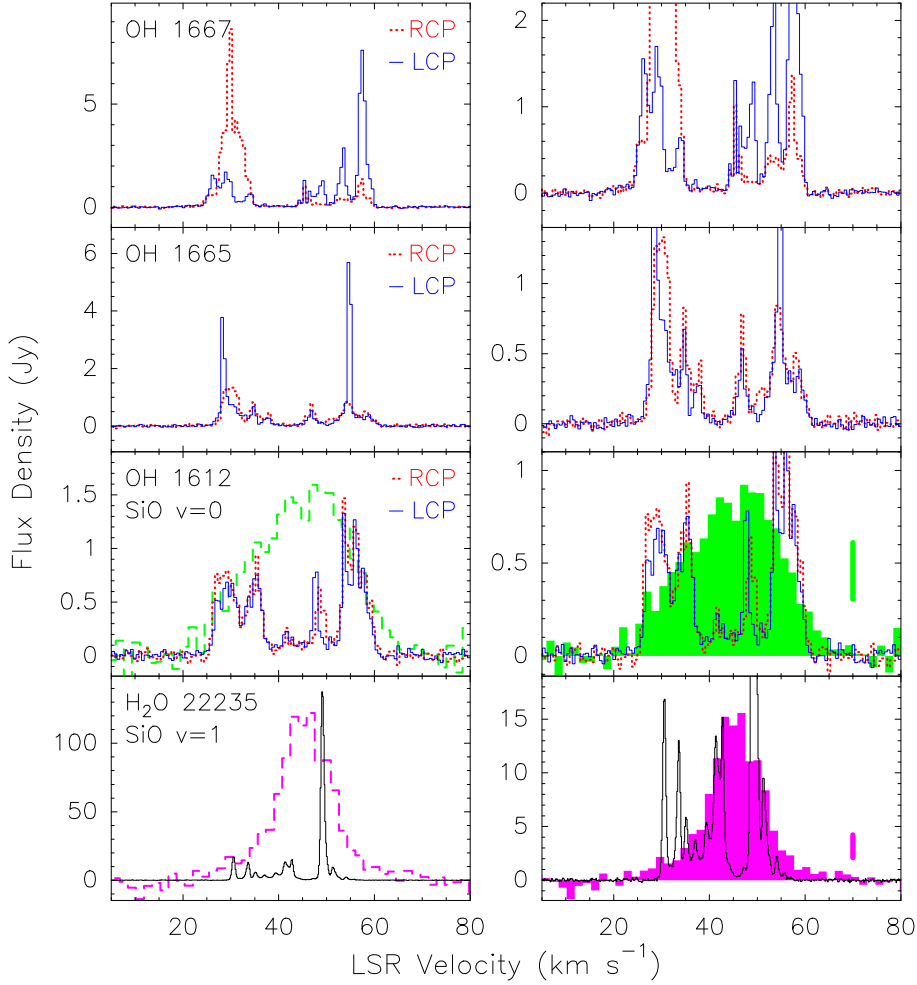


Figure 5. Molecular lines observed toward IRC –10414: The left column shows, bottom to top, spectra of the 22.2 GHz H₂O and the 1612, 1665 and 1667 MHz OH maser transitions taken with the Effelsberg 100 m telescope. For the OH lines, the LCP and RCP spectra shown as full and dotted lines, respectively. The H₂O and 1612 MHz OH spectra are overlaid on spectra of the SiO 217.1 GHz $v = 0, J = 5 - 4$ and 215.6 GHz $v = 1, J = 5 - 4$ transitions (in dashed lines respectively). The right column shows the same with the strongest H₂O and OH maser features truncated to emphasize lower intensity emission and the SiO spectra represented as shaded areas. The vertical bars define the flux density scale for the SiO lines and correspond, in both cases, to 1 Jy.

from an even more compact region. This is clear from the densities and temperatures required for its excitation (see above). With the caveat that their spectra were taken 30 yr apart, we note that the $v = 1, J = 2 - 1$ line observed by Ukita & Goldsmith (1984) in 1982 April was roughly twice as strong as the $v = 1, J = 5 - 4$ one when we observed it. This is in line with the findings of Jewell et al. (1987) who find for a diverse sample of 18 Miras and RSGs flux ratios between 1 and 50. We note that, in contrast to IRC –10414, all the spectra shown for the $v = 1, J = 2 - 1$ and $J = 5 - 4$ lines by Jewell et al. are dominated by one or a few narrow features. For the $v = 1, J = 2 - 1$ line toward IRC –10414, Ukita & Goldsmith (1984) observe a similarly smooth (but noisier) shape we do for the $v = 1, J = 5 - 4$ line, while a more complex profile for the $v = 1, J = 2 - 1$ line (smooth with a narrower peak) was observed by Imai, Deguchi & Miyoshi (1999), who also present spectra of the $v = 1$ and 2, $J = 1 - 0$ lines (the latter being uncharacteristically weak).

Remarkably, the H₂O maser line and the OH main (1665 and 1667 MHz) and satellite (1612 MHz) hfs lines all

cover a similar velocity range, i.e. $2v_{\infty}$, with a large number of narrow maser features. All three of the OH lines show narrow emission features over the velocity range and enhanced emission at high and low velocities, close to $\pm v_{\infty}$. In contrast, the vast majority of 1612 MHz spectra of typical OH/IR stars are characterised by two strong spikes at $\pm v_{\infty}$ with a steady drop off toward the center of the double-peaked profile and an emission minimum at v_{LSR} . Almost all of the 286 OH/IR stars detected in their VLA survey, for which Sevenster et al. (2001) show spectra, have this appearance. Although the low signal-to-noise ratio is an issue for some sources, by visual inspection of their fig. 10 we only find about 10 sources with more than two features (and 10 are single-featured). In contrast, our much higher quality 1612 MHz spectrum of IRC –10414 rivals in complexity that of the “classical” OH/IR red super (or even hyper) giants VY CMa, VX Sgr and IRC +10420 (see Cohen et al. 1987 for high quality/high resolution spectra of these sources). These sources have v_{∞} of 25 to 50 km s⁻¹. The terminal wind velocity of IRC –10414 of 21 km s⁻¹ is somewhat smaller than

these values, but larger than the median v_∞ of 15 km s^{-1} determined by Sevenster et al. (2001) for their sample of OH/IR stars.

In the bands covering the SiO $J = 7 - 6$ lines, we also detect weak emission from two SO lines. Since their level energies above the ground state are similar and because of the limited signal-to-noise ratios of their spectra, it is not possible to use these lines' ratio for calculating a rotation temperature. SO is a well known chemical constituent of the circumstellar envelopes of RSGs and O-rich AGB stars (Sahai & Wannier 1992; Omont et al. 1993; Tenebaum et al. 2010).

In summary, the complexity and width of the maser spectra observed for IRC-10414 support the RSG nature of the star.

6 DISCUSSION

6.1 IRC-10414

6.1.1 Parameters of IRC-10414

Interpolation of the new effective temperature, T_{eff} , scale of Galactic RSGs by Levesque et al. (2005) to M7 supergiants gives $T_{\text{eff}} \approx 3300 \text{ K}$ for IRC-10414. This figure agrees well with that derived from the relation between T_{eff} and the spectral type of G-M-type supergiants (van Belle, Creech-Eakman & Hart 2009):

$$T_{\text{eff}} = -(123 \pm 25)SpT + (4724 \pm 175) \text{ K}, \quad (2)$$

where $SpT=6\dots 14$ correspond to M0...M8, which for M7 stars ($SpT = 13$) gives $T_{\text{eff}} = 3125 \pm 369 \text{ K}$.

With $T_{\text{eff}} = 3300 \text{ K}$, one can calculate the intrinsic $(J - K)_0$ colour of IRC-10414 and its bolometric K -band correction, BC_K , using the relations (Levesque et al. 2005):

$$(J - K)_0 = 3.10 - 0.547(T_{\text{eff}}/1000 \text{ K}) \quad (3)$$

and

$$BC_K = 5.574 - 0.7589(T_{\text{eff}}/1000 \text{ K}), \quad (4)$$

which give $(J - K)_0 = 1.29 \text{ mag}$ and $BC_K = 3.07 \text{ mag}$. Then, using equations (3) and (4), and the J and K_s magnitudes from Table 1, one can estimate the K -band extinction towards the star, its K -band absolute magnitude, and the bolometric luminosity:

$$A_K = 0.66[(J - K) - (J - K)_0], \quad (5)$$

$$M_K = K - DM - A_K, \quad (6)$$

$$\log(L/L_\odot) = 0.4(4.74 - M_K - BC_K), \quad (7)$$

where $K = K_s + 0.04 \text{ mag}$ (Carpenter 2001) and DM is the distance modulus ($DM \approx 11.51 \text{ mag}$ for $d = 2 \text{ kpc}$). For $J = 2.845 \text{ mag}$ and $K_s = 0.713 \text{ mag}$, one has $A_K \approx 0.53 \text{ mag}$ (which corresponds to the visual extinction of $A_V \approx 5 \text{ mag}$; Rieke & Lebofsky 1985), $M_K \approx -11.3 \text{ mag}$ and $\log(L/L_\odot) \approx 5.2$. Depending on the initial rotation velocity of IRC-10414, the derived luminosity corresponds to an initial (zero-age main-sequence) mass of the star of $M \sim 20 - 25 M_\odot$ and implies an age of $\sim 6 - 10 \text{ Myr}$ (Ekström et al. 2012).

M_K can also be estimated from the period- M_K relations of RSGs proposed by Kiss, Szabó & Bedding (2006)

and Yang & Jiang (2012). Using these relations and assuming that $P = 768.16 \text{ d}$ is the fundamental mode of radial pulsation⁴, one finds the mean value of $M_K \approx -11.4 \text{ mag}$. One can also estimate the luminosity of IRC-10414 using empirical period-luminosity relation for semi-regular supergiant variables by Turner et al. (2006; see their fig. 9), which yields $\log(L/L_\odot) \approx 5.2$. The good agreement of these estimates with those derived from equations (5)–(7) provides support for our choice of $d = 2 \text{ kpc}$.

Then, using the luminosity-radius-temperature relation by Levesque et al. (2007):

$$R/R_\odot = (L/L_\odot)^{0.5} (T_{\text{eff}}/5770 \text{ K})^{-2},$$

one finds the radius of IRC-10414 of $R \approx 1200 R_\odot$, which makes it one of the biggest known stars (cf. Wing 2009). For this radius and $M = 20 - 25 M_\odot$, one finds $\log g \approx -(0.3 \div 0.4)$ (cf. Section 4.2). It is also instructive to use these M and R and the period-radius-mass relation for pulsating stars by Gough, Ostriker & Stobie (1965),

$$P \approx 10^{-2} \text{ d} (R/R_\odot)^2 (M/M_\odot)^{-1},$$

to derive the expected period of pulsations of IRC-10414, $P \approx 600 - 700 \text{ d}$, which agrees with our choice of $P = 768.16 \text{ d}$ as the fundamental mode of radial pulsations of IRC-10414.

Recently, Davies et al. (2013) showed that T_{eff} of RSGs derived from optical and near-infrared spectral energy distributions might be significantly (by several hundreds of K) warmer than those based on the T_{eff} scale by Levesque et al. (2005). Adopting $T_{\text{eff}} = 3700 \text{ K}$ for IRC-10414 and using equations (3)–(7), one finds $M_{\text{bol}} = -8.66 \text{ mag}$ and $\log(L/L_\odot) = 5.4$. This higher luminosity, however, would be difficult to reconcile with the moderate \dot{M} derived for IRC-10414 in Section 6.1.3.

6.1.2 IRC-10414 as a runaway

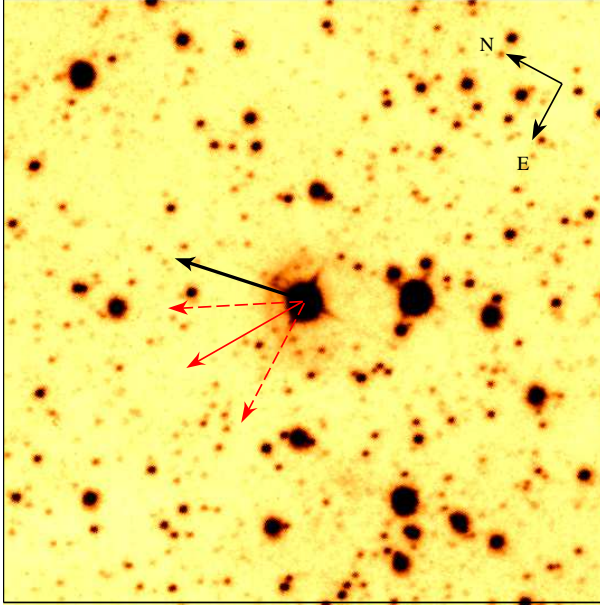
The bow shock interpretation of the arc-like nebula implies that IRC-10414 is moving supersonically with respect to the local ISM. To estimate the peculiar (space) velocity of IRC-10414 and thereby to check its runaway status, we searched for proper motion measurements for this star using the VizieR catalogue access tool⁵. We found several measurements of which the most recent one (and the one with the smallest claimed errors) is provided by the fourth U.S. Naval Observatory CCD Astrograph Catalog (UCAC4; Zacharias et al. 2013). This measurement is given in Table 4 along with the heliocentric radial velocity (as measured in Section 5.2), the components of the peculiar transverse velocity (in Galactic coordinates), v_l and v_b , the peculiar radial velocity, v_r , and the total space velocity, v_* , of the star. To derive these velocities, we used the Galactic constants $R_0 = 8.0 \text{ kpc}$ and $\Theta_0 = 240 \text{ km s}^{-1}$ (Reid et al. 2009) and the solar peculiar motion $(U_\odot, V_\odot, W_\odot) = (11.1, 12.2, 7.3) \text{ km s}^{-1}$

⁴ Note that the long secondary period of 2726.43 d (detected in the light curve of IRC-10414 by Richards et al. 2012) might correspond to the convective turnover time of giant convection cells in the stellar envelope (Stothers & Leung 1971; Kiss et al. 2006).

⁵ <http://webviz.u-strasbg.fr/viz-bin/VizieR>

Table 4. Proper motion, heliocentric radial velocity, peculiar transverse (in Galactic coordinates) and radial velocities, and the total space velocity of IRC –10414.

$\mu_\alpha \cos \delta$ (mas yr ⁻¹)	μ_δ (mas yr ⁻¹)	$v_{r,\text{hel}}$ (km s ⁻¹)	v_l (km s ⁻¹)	v_b (km s ⁻¹)	v_r (km s ⁻¹)	v_* (km s ⁻¹)
5.4 ± 2.9	1.6 ± 2.4	28.6 ± 2.0	53.9 ± 23.9	-30.8 ± 26.5	20.6 ± 2.0	65.4 ± 23.3

**Figure 6.** SHS image of IRC –10414 and its bow shock. The thin (red) arrow shows the direction of motion of the star as suggested by the proper motion measurement (with 1 sigma uncertainties shown by dashed arrows). The thick (black) arrow shows the symmetry axis of the bow shock. See text for details.

(Schönrich, Binney & Dehnen 2010). For the error calculation, only the errors of the proper motion and the radial velocity measurements were considered. The obtained space velocity of $\approx 70 \pm 20 \text{ km s}^{-1}$ implies that IRC –10414 is a classical runaway star (e.g. Blaauw 1961).

Fig. 6 shows that the vector of the peculiar (transverse) velocity is misaligned with the symmetry axis of the bow shock. This misalignment might be caused by inaccuracy of the proper motion measurement or by the effect of a regular flow in the local ISM. The latter explanation is less likely because it requires the presence of gas flowing with a velocity of several tens of km s^{-1} . Such high-velocity flows could be found in the close vicinity of star clusters (e.g. Bally et al. 2006; Povich et al. 2008; Kobulnicky, Gilbert & Kiminki 2010), but they should be rare in the field. The quite large margin of error in velocity components (see Table 4) leaves the possibility that IRC –10414 is moving almost parallel to the Galactic plane (in the direction of growing Galactic longitude), which is suggested by the orientation of the symmetry axis of the bow shock as well. From Table 4 it follows that IRC –10414 is moving away of us and that the vector of its space velocity makes an angle of $\approx 18_{-6}^{+13}$ degrees with respect to the plane of the sky. Thus, the inclination of the bow shock does not much affect our estimate of R_{SO} given in Section 3 (see Gvaramadze et al. 2011c for details).

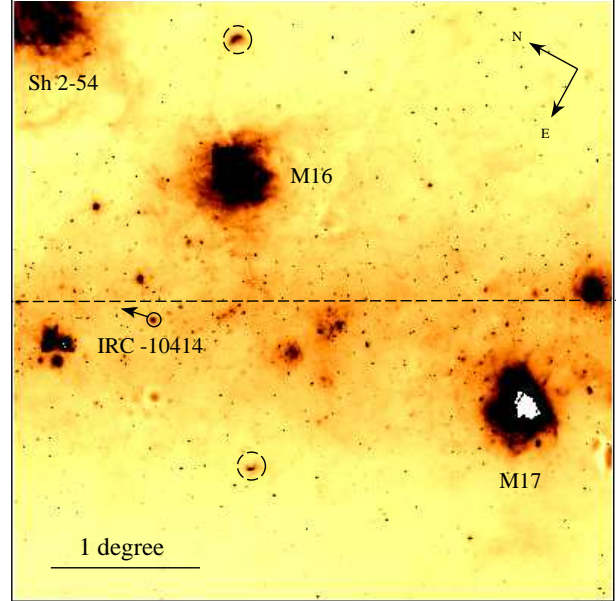
**Figure 7.** $4^\circ \times 4^\circ$ WISE $22 \mu\text{m}$ image of the field containing IRC –10414 and three young massive star clusters NGC 6604, NGC 6611 and NGC 6618, embedded in the H II regions Sh 2-54, M16 and M17, respectively (the latter H II region is highly saturated). The position of IRC –10414 is marked by a circle. The arrow shows the direction of motion of IRC –10414, as suggested by the symmetry axis of the bow shock (see Fig. 6). Two bow shocks produced by O stars running away from NGC 6611 (Gvaramadze & Bomans 2008) are indicated by dashed circles. The Galactic plane is shown by a dashed line. See text for details. At a distance of 2 kpc, 1 degree corresponds to ≈ 34.4 pc.

Fig. 7 shows the $4^\circ \times 4^\circ$ WISE $22 \mu\text{m}$ image⁶ of the Galactic plane centred at $l = 16^\circ.5$, $b = 0^\circ$, with three prominent H II regions, Sh 2-54, M16 and M17, and their central star clusters, NGC 6604, NGC 6611 and NGC 6618, respectively. All three clusters are located at about the same distance of ≈ 2 kpc (Reipurth 2008; Hillenbrand et al. 1993; Xu et al. 2011) and are believed to originate from the same giant molecular cloud (Sofue et al. 1986). In Fig. 7 we indicate by dashed circles the positions of two bow-shock-producing O stars. Proper motion measurements for these stars and the orientations of their bow shocks are consistent with the possibility that both stars are running away from NGC 6611 (Gvaramadze & Bomans 2008). Although the past trajectory of IRC –10414 (inferred from the orientation of the peculiar transverse velocity of this star) might intersect the trajectory of NGC 6611 as well (see fig. 1 in Gvaramadze & Bomans 2008), we note that the age of the cluster is a fac-

⁶ The image was generated by the NASA’s SkyView facility (McGlynn, Scollick & White 1996).

tor of $\approx 2 - 3$ younger than that of the star (Gvaramadze & Bomans 2008 and references therein), which implies that NGC 6611 cannot be the birth place of IRC-10414. Instead, assuming that the symmetry axis of the bow shock better reflects the direction of motion of the star, one can infer that IRC-10414 is moving away from M17.

It is, however, unlikely that M17 is the birth place of IRC-10414 because the central cluster of this H II region, NGC 6618, is very young (~ 1 Myr; Chini & Hoffmeister 2008). One can therefore suggest that IRC-10414 has been ejected from the more distant stellar system, e.g. from the Sgr OB4 association (Humphreys 1978), which is located further southwest of M17 (at ≈ 5.5 or ≈ 190 pc in projection from IRC-10414) and whose distance from the Sun is also ≈ 2 kpc (e.g. Mel'nik & Dambis 2009). In this case, the ejection event must have happened $\approx 3.5_{-1.1}^{+2.8}$ Myr ago, provided that the peculiar transverse velocity of IRC-10414 is $\approx v_l$ (see Table 4). The birth place of IRC-10414 might even be more distant ($\approx 9 - 15$ degrees) if this 6–10 Myr old star was ejected dynamically at the very beginning of dynamical evolution of its parent stellar system.

Finally, one cannot exclude the possibility that IRC-10414 was a member of a runaway binary or hierarchical triple system, which was dissolved either because of supernova explosion of one of the binary components (Pflamm-Altenburg & Kroupa 2010) or evolution of the most massive members of the triple (Gvaramadze & Menten 2012). In both cases, IRC-10414 cannot be traced back to its parent star cluster (cf. Gvaramadze et al. 2012), while in the second one, WR 114 might be the former member of the dissolved triple system⁷. Dissolution of the triple system would cause IRC-10414 and WR 114 to move in the opposite directions to each other, but this cannot be proved at present because the existing proper motion measurements for WR 114 are highly unreliable.

6.1.3 Mass-loss rate of IRC-10414

Now we use v_* derived in Section 6.1.2 and the upper limit on n_e obtained in Section 6.2 to estimate \dot{M} of IRC-10414.

First, we use n_e to constrain the preshock number density, n_0 , i.e. the number density of the local ISM. For this we use an empirical relation between the [S II] electron number density and the shock velocity v_{sh} (Dopita 1978):

$$n_0 \approx 0.02 n_e \left(\frac{v_{sh}}{100 \text{ km s}^{-1}} \right)^{-2}. \quad (8)$$

With $n_e \leq 100 \text{ cm}^{-3}$ and $v_{sh} = v_* = 70 \text{ km s}^{-1}$, one has $n_0 \leq 5 \text{ cm}^{-3}$.

Then, we express \dot{M} through n_0 and the observables, v_* , R_{SO} and v_∞ :

$$\begin{aligned} \dot{M}_{obs} = 1.0 \times 10^{-5} \text{ M}_\odot \text{ yr}^{-1} & \left(\frac{v_*}{70 \text{ km s}^{-1}} \right)^2 \left(\frac{R_{SO}}{0.14 \text{ pc}} \right)^2 \\ & \times \left(\frac{n_0}{5 \text{ cm}^{-3}} \right) \left(\frac{v_\infty}{21 \text{ km s}^{-1}} \right)^{-1}. \end{aligned}$$

⁷ Note that the VIIth Catalogue of Galactic Wolf-Rayet Stars by van der Hucht (2001) gives for WR 114 a distance of 2 kpc and indicates this star as a possible binary system (see, however, Sander, Hamann & Todt 2012).

This estimate of \dot{M} should be considered as an upper limit because n_0 is constrained only from the upper end. Note also that, according to equation (8), $n_0 \propto v_*^{-2}$, so that formally \dot{M}_{obs} does not depend on the stellar space velocity. In fact, the dependence of n_0 on v_* is more complex because n_e is a function of v_* (or v_{sh}) as well.

It is interesting to compare \dot{M}_{obs} with rates based on various mass-loss prescriptions proposed for RSGs (see Maun & Josselin 2011 for a recent review). Using the recipe by Jura & Kleinmann (1989) and the parameters of IRC-10414, one finds $\dot{M} \approx 2 \times 10^{-5} \text{ M}_\odot \text{ yr}^{-1}$ (cf. Section 2), which is at least a factor of 2 higher than \dot{M}_{obs} .

A lower mass-loss rate follows from the use of the empirical law by de Jager, Nieuwenhuijzen & van der Hucht (1988). For $L = 10^{5.2} L_\odot$ and $T_{eff} = 3300$ K, the de Jager et al.'s prescription predicts $\dot{M} \approx 5 \times 10^{-6} \text{ M}_\odot \text{ yr}^{-1}$ (see fig. 6 in Maun & Josselin 2011). This estimate would be consistent with \dot{M}_{obs} if $n_0 = 2.5 \text{ cm}^{-3}$.

An even lower rate could be derived from the recipe by Verhoelst et al. (2009):

$$\dot{M} = 10^{-16.2 \pm 1.8} (L/L_\odot)^{1.89 \pm 0.36},$$

which gives $\dot{M} = 4.2 \times 10^{-7} \text{ M}_\odot \text{ yr}^{-1}$. Although this estimate would agree with \dot{M}_{obs} for a reasonable number density of the local ISM of $n_0 = 0.2 \text{ cm}^{-3}$, we note that the large spread allowed by the Verhoelst et al.'s recipe leaves the possibility that the actual \dot{M} could be much higher.

\dot{M} of IRC-10414 can also be estimated through the $K_s - [24]$ colour of this star, where [24] is the MIPS $24 \mu\text{m}$ magnitude (see Bonanos et al. 2010 and references therein). The saturation of the MIPS $24 \mu\text{m}$ image of IRC-10414 (see Fig. 1), however, does not allow us to measure [24]. Hence, we use the IRAS $25 \mu\text{m}$ magnitude (Helou & Walker 1988), [25] = -4.213 mag, instead of [24]. Assuming the gas-to-dust ratio of 200 (typical of Galactic RSGs) and using equations (1) and (2) in Bonanos et al. (2010), one finds $\dot{M} = 9.9 \times 10^{-6} \text{ M}_\odot \text{ yr}^{-1}$, which agrees well with \dot{M}_{obs} (provided that $n_0 \approx 5 \text{ cm}^{-3}$).

Finally, \dot{M} can be derived from the prescription by van Loon et al. (2005), according to which \dot{M} increases almost linearly with increasing L and sharply decreases with increase of T_{eff} :

$$\dot{M} = 2.5 \times 10^{-5} \text{ M}_\odot \text{ yr}^{-1} (L/10^5 L_\odot)^{1.05} (T_{eff}/3500 \text{ K})^{-6.3}.$$

For $L = 10^{5.2} L_\odot$ and $T_{eff} = 3300$ K this formulation gives $\dot{M} = 5.9 \times 10^{-5} \text{ M}_\odot \text{ yr}^{-1}$, which is much higher than \dot{M}_{obs} (recall that \dot{M}_{obs} is the upper limit on the mass-loss rate of IRC-10414). Interestingly, the mass-loss rates of both known bow-shock-producing RSGs, Betelgeuse and μCep , are much smaller than those predicted by van Loon et al. (2005) as well.

6.2 Bow shock

6.2.1 Stability

Numerical and analytical studies of bow shocks produced by RSG and other cool stars show that they are unstable to a considerable degree (e.g. Brighenti & D'Ercole 1995; Dgani, van Buren & Noriega-Crespo 1996; Wareing, Zijlstra & O'Brien 2007a,b; van Marle et al. 2011; Mohamed, Mackey & Langer 2012; Cox et al. 2012; Decin et al. 2012). Corre-

spondingly, one can expect that these bow shocks should have a ragged appearance, which is in an obvious conflict with the observed smoothness of bow shocks associated with Betelgeuse and IRC –10414.

A possible solution proposed by Mohamed et al. (2012) is that younger bow shocks are more stable (because all instabilities have a finite growth timescale), so a very smooth bow shock can be an indication of its youth. If the bow shock is young then it is likely moving into gas from previous mass-loss phases, so the circumstellar gas could already be enriched in elements such as nitrogen. Mackey et al. (2012) showed that a BSG evolving into a RSG would have a low-mass bow shock expanding into ionized BSG wind material for a short time ($\approx 20\,000$ years) after the star evolves to a RSG. It is possible but unlikely that we observe IRC –10414 in just this phase of evolution.

It should be noted that in the above-mentioned papers, the stellar wind was considered to be neutral (which is natural for cool, RSG and AGB, stars), while the ISM was assumed to be either neutral or ionized. Also, numerical modelling of bow shocks generated by hot stars in the ionized ISM show that they are stable for certain v_* and \dot{M} (e.g. Comerón & Kaper 1998; Meyer et al., in preparation). Thus, one can suppose that the smooth shape of the bow shocks generated by IRC –10414 and Betelgeuse is because the wind of these stars and their ambient ISM are both ionized. This supposition can be supported by the following considerations.

Mohamed et al. (2012) found that their simulated bow shocks were much less stable than those of Wareing et al. (2007a) for similar wind and ISM parameters. The only physical difference in the models was that Wareing et al. (2007) assumed “an unphysical temperature of 10^4 K” for the stellar wind, whereas Mohamed et al. (2012) allowed gas to cool to lower temperatures. Mohamed et al. proposed that the greater compression caused by the cooling in their simulations made the bow shock thinner and therefore less stable. Proceeding from this, one can expect that if the wind and ISM are both photoionized, so that their temperature is kept at $T \approx 10^4$ K and thereby prevented from cooling to lower temperatures, then the bow shock would be more stable than a bow shock that is not photoionized. This will be studied in more detail for the bow shock of IRC –10414 by Meyer et al. (in preparation).

While an ionized ISM is the most widespread component of the ISM (McKee & Ostriker 1977), the assumption that the wind of IRC –10414 is ionized is less trivial because this star is too cool to ionize the wind material by itself. The wind of IRC –10414 could be ionized (at least partially) if this star forms a binary system with a hot massive star or a compact object. Such a situation takes place in the case of α Sco (Antares), which is composed of M1 Iab and B3 V: stars (Kudritzki & Reimers 1978; Reimers et al. 2008). In the absence of data supporting the possible binarity of IRC –10414, we consider an alternative possibility, namely that the wind of this star is ionized by an external source of ionizing photons (see next section). A good evidence supporting this possibility is the presence of the very strong [N II] emission in the spectrum of the bow shock (Section 4.3), which means that the stellar wind is ionized to a significant degree. Since the wind material cannot be collisionally ionized because the reverse shock is too weak, it is

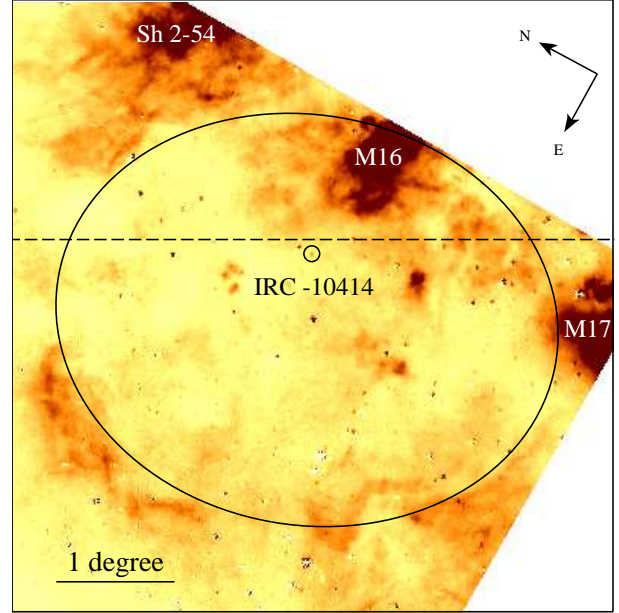


Figure 8. SHASSA continuum-subtracted image of the field containing IRC –10414 (marked by a circle) and three young massive star clusters, NGC 6604, NGC 6611 and NGC 6618, embedded in the H II regions, Sh 2-54, M16 and M17, respectively. The putative ionization-bounded H II region created by NGC 6611 is outlined by an ellipse. The Galactic plane is shown by a dashed line. See text for details. At a distance of 2 kpc, 1 degree corresponds to ≈ 34.4 pc.

natural to assume that it is photoionized by some external source(s).

6.2.2 Ionization source

The close angular proximity between IRC –10414 and WR 114 prompted us to consider the possibility that the latter star photoionizes the wind of the former one (recall that the distance to WR 114 is 2 kpc).

Following Morris & Jura (1983), we can calculate the stand-off radius of the ionization front, R_i , in the RSG wind (i.e. the minimum distance from the ionization front to the RSG star) as a function of the incident ionizing radiation field:

$$R_i = 0.01 \text{ pc} \left(\frac{\dot{M}}{2 \times 10^{-6} \text{ M}_{\odot} \text{ yr}^{-1}} \right)^{2/3} \times \left(\frac{v_{\infty}}{21 \text{ km s}^{-1}} \right)^{-2/3} \left(\frac{F_{\gamma}}{10^{10} \text{ cm}^{-2} \text{ s}^{-1}} \right)^{-1/3}, \quad (9)$$

where F_{γ} is the ionizing photon flux. For a point source of ionizing photons $F_{\gamma} = L_{\gamma}/(4\pi l^2)$, where L_{γ} is the ionizing photon luminosity of the source and l is the linear separation between the source and the RSG star.

With $L_{\gamma} = 10^{48.9} \text{ s}^{-1}$ (Crowther 2007) for a WC5 star like WR 114, and assuming that l is equal to the projected distance between the two stars, i.e. $l \approx 0.43$ pc, one finds $F_{\gamma} \approx 3.6 \times 10^{11} \text{ s}^{-1} \text{ cm}^{-2}$ and $R_i \approx 3.4 \times 10^{-3}$ pc or $\approx 0.02 R_{\text{SO}}$ (i.e. WR 114 can, in principle, ionize very deep layers of the wind of IRC –10414). But such a small separation between IRC –10414 and WR 114 is unlikely because the strong wind of the later star would prevent formation

of the bow shock around the former one. Thus, the separation between the two stars should at least be as large as the characteristic scale of the wind-bubble created by WR 114, i.e. (Weaver et al. 1977):

$$R_b = 27 \text{ pc} \left(\frac{L_w}{10^{36} \text{ erg s}^{-1}} \right)^{1/5} \left(\frac{n_0}{1 \text{ cm}^{-3}} \right)^{-1/5} \left(\frac{t}{1 \text{ Myr}} \right)^{3/5},$$

where $L_w = \dot{M}v_\infty^2/2$ is the mechanical luminosity of the star and t is the age of the bubble. With $\dot{M} = 2.9 \times 10^{-5} M_\odot \text{ yr}^{-1}$ and $v_\infty = 3200 \text{ km s}^{-1}$ (Sander et al. 2012) and assuming $t = 0.5 \text{ Myr}$, we obtain $L_w \approx 9.4 \times 10^{37} \text{ erg s}^{-1}$ and $R_b \approx 44 \text{ pc}$. For $l \geq R_b$, one finds $R_i \geq 0.4R_{\text{SO}}$, i.e. WR 114 still could be the ionization source of the wind of IRC–10414.

Another possibility is that the wind of IRC–10414 is ionized by the star cluster NGC 6611 (cf. Morris & Jura 1983), which is located at $\approx 38 \text{ pc}$ in projection from IRC–10414. Using the census of massive stars in NGC 6611 from Evans et al. (2005) and calibration of stellar parameters of Galactic O stars from Martins et al. (2005), we estimated the total ionizing photon luminosity of the cluster to be $L_\gamma(\text{NGC 6611}) \approx 10^{50} \text{ s}^{-1}$ (cf. Hester et al. 1996). Assuming that $l = 38 \text{ pc}$ and neglecting attenuation of the ionizing flux by photoelectric absorption in the ISM, one finds $F_\gamma \approx 5.8 \times 10^8 \text{ s}^{-1} \text{ cm}^{-2}$. Then using equation (9), we obtain $R_i \approx 0.03 \text{ pc}$ or $\approx 0.2R_{\text{SO}}$, i.e. NGC 6611 could be the ionization source of the wind of IRC–10414 as well.

The high L_γ of NGC 6611 might also be responsible for creation of an extended H II region to the east-southeast of IRC–10414. The characteristic scale of this H II region should be of the same order of magnitude as the Strömgren radius, which is given by (e.g. Lequeux 2005):

$$R_s = 140 \text{ pc} \left(\frac{L_\gamma}{10^{50} \text{ s}^{-1}} \right)^{1/3} \left(\frac{n_0}{1 \text{ cm}^{-3}} \right)^{-2/3}.$$

Indeed, inspection of the Southern H-alpha Sky Survey Atlas (SHASSA; Gaustad et al. 2001) revealed an $\approx 2.7^\circ \times 3.3^\circ$ structure (outlined in Fig. 8 by an ellipse). The linear size of this structure of $\approx 90 \times 110 \text{ pc}$ approximately agrees with R_s , which suggests that it might be the *ionization-bounded* H II region produced by NGC 6611 (as distinct from the *density-bounded* blister-like H II region M16).

To conclude, we note that if the wind of IRC–10414 is ionized by a single ionizing source and if R_i constitutes a non-negligible fraction of R_{SO} (see above), then one can expect to see a comet-like tail of H I gas attached to the star and pointed away from the source of ionization. Interestingly, observations of Betelgeuse in the H I line at 21 cm by Le Bertre et al. (2012) revealed such a tail in the direction opposite to the star’s space motion. This detection may imply that Betelgeuse is moving towards the ionizing source and suggests that the stability of the bow shock around this star could be because a part of the stellar wind is ionized. Similar observations of IRC–10414, however, appear to be practically impossible, because of the much larger distance to this star and contamination with H II emission in the Galactic plane.

7 SUMMARY

In this paper, we presented the discovery of an optically visible arc-like nebula around the late M star IRC–10414

using the SuperCOSMOS H-alpha Survey. We also reported the results of follow-up spectroscopy of IRC–10414 and its nebula with the Southern African Large Telescope (SALT). We have classified IRC–10414 as an M7 supergiant, thereby confirming previous claims on the red supergiant (RSG) nature of this star based on observations of its maser emission. The RSG nature of IRC–10414 was further supported by our new radio- and (sub)millimeter-wavelength molecular line observations made with the Atacama Pathfinder Experiment (APEX) 12 meter telescope and the Effelsberg 100 m radio telescope, respectively. We detected maser emission from OH, H₂O and SiO, as well as thermally excited emission from the latter and from SO. These observations also yield the star’s local-standard of rest velocity of $43 \pm 2 \text{ km s}^{-1}$ and the wind terminal velocity of $21 \pm 2 \text{ km s}^{-1}$.

Using the recent proper motion measurement for IRC–10414, we estimated the space velocity of this star to be $\approx 70 \pm 20 \text{ km s}^{-1}$, which implies that IRC–10414 is a classical runaway. This finding along with the arc-like shape of the nebula suggest that the nebula is a bow shock. The bow shock interpretation was reinforced by the SALT spectrum of the nebula, which yields the [S II] $\lambda\lambda 6716, 6731/\text{H}\alpha$ ratio of 0.4, typical of shock-excited nebulae. From intensities of the [N II] and [S II] lines detected in the spectrum of the bow shock we found that the line-emitting material is enriched in nitrogen. We considered this as an indication that the bow shock emission at least partially originates in the shocked stellar wind, which in RSGs is overabundant in nitrogen because of the dredge-up of the nuclear processed gas. Detection of the bow shock around IRC–10414 makes this star the third case of bow-shock-producing RSGs (with two other cases being Betelgeuse and μ Cep) and the first one with a bow shock visible in the optical range.

The spectroscopy of the bow shock also allowed us to constrain the number density of the local ISM, which along with the stand-off distance of the bow shock and the wind and space velocities of the star provide an estimate of the mass-loss rate of IRC–10414. This estimate was compared with mass-loss rates based on various prescriptions proposed for RSGs.

We discussed the smooth appearance of the bow shocks around IRC–10414 and Betelgeuse and suggested that one of the necessary conditions for stability of bow shocks generated by RSG and other cool stars is the ionization of the stellar wind. Possible ionization sources of the wind of IRC–10414 were proposed and discussed.

8 ACKNOWLEDGEMENTS

AYK acknowledges the support from the National Research Foundation (NRF) of South Africa. JM is funded by a fellowship from the Alexander von Humboldt Foundation. We are grateful to E.M. Levesque for useful discussion. This work was partly based on observations with the Southern African Large Telescope (SALT) and the 100-m telescope of the Max-Planck-Institut für Radioastronomie at Effelsberg, and supported by the Deutsche Forschungsgemeinschaft priority program 1573, Physics of the Interstellar Medium. It also has made use of the NASA/IPAC Infrared Science Archive, which is operated by the Jet Propulsion Laboratory, Cali-

fornia Institute of Technology, under contract with the National Aeronautics and Space Administration, the Southern H-Alpha Sky Survey Atlas (SHASSA), which is supported by the National Science Foundation, the SIMBAD data base and the VizieR catalogue access tool, both operated at CDS, Strasbourg, France.

REFERENCES

- Asplund M., Grevesse N., Sauval A.J., Scott P., 2009, *ARA&A*, 47, 481
- Baars J.W.M., Genzel R., Pauliny-Toth I.I.K., Witzel A., 1977, *A&A*, 61, 99
- Bally J., Licht D., Smith N., Walawender J., 2006, *AJ*, 131, 473
- Blaauw A., 1961, *Bull. Astron. Inst. Netherlands*, 15, 265
- Beauchamp A., Moffat A.F.J., Drissen L., 1994, *ApJSS*, 93, 187
- Benaglia P., Romero G.E., Marti J., Peri C.S., Araudo A.T., 2010, *A&A*, 517, L10
- Benjamin R.A. et al., 2003, *PASP*, 115, 953
- Benvenuti P., D'Odorico S., Peimbert M., 1973, *A&A*, 28, 447
- Blommaert J.A.D.L., van Langevelde H.J., Michiels W.F.P., 1994, *A&A*, 287, 479
- Bonanos A.Z. et al., 2010, *AJ*, 140, 416
- Brighenti F., D'Ercole A., 1995, *MNRAS*, 277, 53
- Brogan C.L., Gelfand J.D., Gaensler B.M., Kassim N.E., Lazio T.J.W., 2006, *ApJ*, 639, L25
- Brott I. et al., 2011, *A&A*, 530, A115
- Buckley D.A.H., Swart G.P., Meiring J.G., 2006, *SPIE*, 6267, 32
- Bujarrabal V., 1994, *A&A*, 285, 971
- Burgh E.B., Nordsieck K.H., Kobulnicky H.A., Williams T.B., O'Donoghue D., Smith M.P., Percival J.W., 2003, *SPIE*, 4841, 1463
- Carey S.J. et al., 2009, *PASP*, 121, 76
- Carpenter J.M., 2001, *AJ*, 121, 2851
- Chapman J.M., Cohen R.J., 1986, *MNRAS*, 220, 513
- Chini R., Hoffmeister V., in Reipurth B. ed., *Handbook of Star Forming Regions, Volume II: The Southern Sky*. Astron. Soc. Pac., San Francisco, p. 625
- Cohen R.J., Down G., Emerson R., Grimm M., Gulkis S., Stevens G., Tarter J., 1987, *MNRAS*, 225, 491
- Comerón F., Kaper L., 1998, *A&A*, 338, 273
- Cox N.L.J. et al., 2012, *A&A*, 537, A35
- Crawford S.M. et al., 2010, *SPIE*, 7737
- Crowther P.A., 2007, *ARA&A*, 45, 177
- Cutri R.M. et al., 2003, *VizieR Online Data Catalog*, 2246, 0
- Davies B. et al., 2013, *ApJ*, 767, 3
- Dgani R., van Buren D., Noriega-Crespo A., 1996, *ApJ*, 461, 927
- de Jager C., Nieuwenhuijzen H., van der Hucht K.A., 1988, *A&AS*, 72, 259
- Decin L. et al., 2012, *A&A*, 548, A113
- Dopita M.A., 1978, *ApJS*, 37, 117
- Ekström S. et al., 2012, *A&A*, 537, A146
- Engels D., 1979, *A&AS*, 36, 337
- Esteban C., Vilchez J.M., Manchado A., Smith L.J., 1991, *A&A*, 244, 205
- Evans C.J. et al., 2005, *A&A*, 437, 467
- Fazio G.G. et al., 2004, *ApJS*, 154, 10
- Fesen R.A., Blair W.P., Gull T.R., 1981, *ApJ*, 245, 131
- Fesen R.A., Blair W.P., Kirshner R.P., 1985, *ApJ*, 292, 29
- Gaustad J.E., McCullough P.R., Rosing W., van Buren D., 2001, *PASP*, 113, 1326
- Gies D.R., Bolton C.T., 1986, *ApJS*, 61, 419
- Gough D.O., Ostriker J.P., Stobie R.S., 1965, *ApJ*, 142, 1649
- Gull T.R., Sofia S., 1979, *ApJ*, 230, 782
- Güsten R., Nyman L.Å., Schilke P., Menten K., Cesarsky C., Booth R., 2006, *A&A*, 454, L13
- Gvaramadze V.V., 2009, *MNRAS*, 395, L85
- Gvaramadze V.V., Bomans D.J., 2008, *A&A*, 490, 1071
- Gvaramadze V.V., Menten K.M., 2012, *A&A*, 541, A7
- Gvaramadze V.V., Gualandris A., Portegies Zwart S., 2009, *MNRAS*, 396, 570
- Gvaramadze V.V., Kroupa P., Pflamm-Altenburg J., 2010, *A&A*, 519, A33
- Gvaramadze V.V., Pflamm-Altenburg J., Kroupa P., 2011a, *A&A*, 525, A17
- Gvaramadze V.V., Kniazev A.Y., Chené A.-N., Schnurr O., 2013, *MNRAS*, 430, L20
- Gvaramadze V.V., Kniazev A.Y., Kroupa P., Oh S., 2011b, *A&A*, 535, A29
- Gvaramadze V.V., Röser S., Scholz R.-D., Schilbach E., 2011c, *A&A*, 529, A14
- Gvaramadze V.V., Weidner C., Kroupa P., Pflamm-Altenburg J., 2012, *MNRAS*, 424, 3037
- Habing H.J., 1996, *A&ARv*, 7, 97
- Hansen O.L., Blanco V.M. 1975, *AJ*, 80, 1011
- Helfand D.J., Becker R.H., White R.L., Fallon A., Tuttle S., 2006, *AJ*, 131, 2525
- Helou G., Walker D.W., 1988, *Infrared Astronomical Satellite (IRAS) Catalogs and Atlases, Vol. 7*. NASA, Washington, DC
- Henney W.J., Arthur S.J., Williams R.J.R., Ferland G.J., 2005, *ApJ*, 621, 328
- Hester J.J. et al., 1996, *AJ*, 111, 2349
- Heyminck S., Kasemann C., Güsten R., de Lange G., Graf U.U., 2006, *A&A*, 454, L21
- Hillenbrand L.A., Massey P., Strom S.E., Merrill K.M., 1993, *AJ*, 106, 1906
- Hollis J.M., Oliverson R.J., Wagner R.M., Feibelman W.A., 1992, *ApJ*, 393, 217
- Humphreys R.M., 1978, *ApJS*, 38, 309
- Imai H., Deguchi S., Miyoshi M., 1999, *PASJ*, 51, 587
- Jaschek C., Jaschek M., 1987, *The Classification of Stars*. Cambridge Univ. Press, Cambridge
- Jewell P.R., Dickinson D.F., Snyder L.E., Clemens D.P., 1987, *ApJ*, 323, 749
- Jones J.E., Alloin D.M., Jones B.J.T., 1984, *ApJ*, 283, 457
- Jura M., 1987, *ApJ*, 313, 743
- Jura M., Kleinmann S.G., 1989, *ApJ*, 341, 359
- Kaper L., van Loon J.Th., Augusteyn T., Goudfrooij P., Patat F., Waters L.B.F.M., Zijlstra A.A., 1997, *ApJ*, 475, L37
- Kirshner R.P., Chevalier R.A., 1980, *ApJ*, 242, L77
- Kiss L.L., Szabó G.M., Bedding T.R., 2006, *MNRAS*, 372, 1721
- Klein B., Philipp S.D., Krämer I., Kasemann C., Güsten R., Menten K.M., 2006, *A&A*, 454, L29
- Kleinmann S.G., Sargent D.G., Dickinson D.F., 1978, *AJ*, 83, 1206
- Kniazev A.Y. et al., 2008, *MNRAS*, 388, 1667
- Kniazev A.Y. et al., 2013, *ApJ*, 770, 124.
- Kobulnicky H.A., Gilbert I.J., Kiminki D.C., 2010, *ApJ*, 710, 549
- Kobulnicky H.A., Nordsieck K.H., Burgh E.B., Smith M.P., Percival J.W., Williams T.B., O'Donoghue D., 2003, *SPIE*, 4841, 1634
- Kolena J., Pataki L., 1977, *AJ*, 82, 150
- Krueger T.K., Aller L.H., Czyzak S.J., 1970, *ApJ*, 160, 921
- Kroupa P., Aarseth S., Hurley J., 2001, *MNRAS*, 321, 699
- Kudritzki R.P., Reimers D., 1978, *A&A*, 70, 227
- Kwok S., Volk K., Bidelman W.P., 1997, *ApJS*, 112, 557
- Lada C.J., Lada E.A., 2003, *ARA&A*, 41, 57
- Lada C.J., Blitz L., Reid M.J., Moran J.M., 1981, *ApJ*, 243, 769
- Lamers H.J.G.L.M., Nota A., Panagia N., Smith L.J., Langer N., 2001, *ApJ*, 551, 764
- Le Bertre T., Nyman L.-A., 1990, *A&A*, 233, 477
- Le Bertre T., Matthews L.D., Gérard E., Libert Y., 2012, *MNRAS*, 422, 3433
- Leonard P.J.T., 1991, *AJ*, 101, 562

- Leonidaki I., Boumis P., Zezas A., 2013, MNRAS, 429, 189
- Lequeux J., 2005, *The Interstellar Medium*. Springer, Berlin
- Levesque E.M., Massey P., Olsen K.A.G., Plez B., 2007, ApJ, 667, 202
- Levesque E.M., Massey P., Olsen K.A.G., Plez B., Josselin E., Maeder A., Meynet G., 2005, ApJ, 628, 973
- Lockett P., Elitzur M., 1992, ApJ, 399, 704
- Lockwood G.W., 1985, ApJS, 58, 167
- Longmore A.J. et al., 2011, MNRAS, 416, 465
- López-Santiago J. et al., 2012, ApJ, 757, L6
- Mackey J., Mohamed S., Neilson H.R., Langer N., Meyer D.M.-A., 2012, ApJ, 751, L10
- Maeda T. et al., 2008, PASJ, 60, 1057
- Martins F., Schaerer D., Hillier D.J., 2005, A&A, 436, 1049
- Mauron N., Josselin E., 2011, A&A, 526, A156
- McGlynn T., Scollick K., White N., 1996, in McLean B.J., Golombek D.A., Hayes J.J.E., Payne H.E. eds., *New Horizons from Multi-Wavelength Sky Surveys*, Proc. IAU Symp., 179, 465
- McKee C.F., Ostriker J.P., 1977, ApJ, 218, 148
- Melnik A.M., Dambis A.K., 2009, MNRAS, 400, 518
- Mercer E.P. et al., 2005, ApJ, 635, 560
- Mohamed S., Mackey J., Langer N., 2012, A&A, 541, A1
- Morris M., Jura M., 1983, ApJ, 267, 179
- Noriega-Crespo A., van Buren D., Dgani R., 1997a, AJ, 113, 780
- Noriega-Crespo A., van Buren D., Cao Y., Dgani R., 1997b, AJ, 114, 837
- O'Donoghue D. et al., 2006, MNRAS, 372, 151
- Omont A., Lucas R., Morris M., Guilloteau S., 1993, A&A, 267, 490
- Oskinova L.M., Ignace R., Hamann W.-R., Pollock A.M.T., Brown J.C., 2003, A&A, 402, 755
- Parker Q.A. et al., 2005, MNRAS, 362, 689
- Pavlović M., Urošević D., Vukotić B., Arbutina B., Göker Ü., 2013, ApJS, 204, 4
- Peri C.S., Benaglia P., Brookes D.P., Stevens I.R., Isequilla N.L., 2012, A&A, 538, A108
- Pflamm-Altenburg J., Kroupa P., 2010, MNRAS, 404, 1564
- Phillips J.P., 1998, A&A, 340, 527
- Pierce M.J., Frew D.J., Parker Q.A., Köppen J., 2004, PASA, 21, 334
- Pojmański G., Maciejewski G., 2005, Acta Astron., 55, 97
- Portegies Zwart S.F., 2000, ApJ, 544, 437
- Poveda A., Ruiz J., Allen C., 1967, Bol. Obs. Tonantzintla Tacubaya, 4, 86
- Povich M.S., Benjamin R.A., Whitney B.A., Babler B.L., Indebetouw R., Meade M.R., Churchwell E., 2008, ApJ, 689, 242
- Price S.D., Egan M.P., Carey S.J., Mizuno D.R., Kuchar T.A., 2001, AJ, 121, 2819
- Rappaport S., Chiang E., Kallman T., Malina R., 1994, ApJ, 431, 237
- Reid M.J., Menten K.M., Zheng X.W., Brunthaler A., Xu Y., 2009, ApJ, 705, 1548
- Reimers D., Hagen H.-J., Baade R., Braun K., 2008, A&A, 491, 229
- Reipurth B., 2008, in Reipurth B., ed., *ASP Monograph Publications*, Vol. 5, *Handbook of Star Forming Regions*, Vol. II: *The Southern Sky*. Astron. Soc. Pac., San Francisco, p. 590
- Reynolds R.J., 1985, ApJ, 288, 622
- Richards J.W., Starr D.L., Miller A.A., Bloom J.S., Butler N.R., Brink H., Crellin-Quick A., 2012, ApJS, 203, 32
- Rieke G.H., Lebofsky M.J., 1985, ApJ, 288, 618
- Rieke G.H. et al., 2004, ApJS, 154, 25
- Sahai R., Wannier P.G., 1992, ApJ, 394, 320
- Sander A., Hamann W.-R., Todt H., 2012, A&A, 540, A144
- Saraph H.E., Seaton M.J., 1970, MNRAS, 148, 367
- Schönrich R., Binney J., Dehnen W., 2010, MNRAS, 403, 1829
- Sevenster M.N., van Langevelde H.J., Moody R.A., Chapman J.M., Habing H.J., Killeen N.E.B., 2001, A&A, 366, 481
- Sharpless S., 1956, ApJ, 124, 342
- Smith L.F., 1968, MNRAS, 138, 109
- Smith L.J., Stroud M.P., Esteban C., Vilchez J.M., 1997, MNRAS, 290, 265
- Sofue Y., Handa T., Fuerst E., Reich W., Reich P., 1986, PASJ, 38, 347
- Solf J., 1978, A&AS, 34, 409
- Stone R.C., 1991, AJ, 102, 333
- Stothers R., Leung K.C., 1971, A&A, 10, 290
- Stupar M., Parker Q.A., 2009, MNRAS, 394, 1791
- Tenenbaum E.D., Dodd J.L., Milam, S.N., Woolf, N.J., Ziurys L.M., 2010, ApJS, 190, 348
- Turner D.G., Rohanizadegan M., Berdnikov L.N., Pastukhova E.N., 2006, PASP, 118, 1533
- Turnshek D.E., Turnshek D.A., Craine E.R., Boeshaar P.C., 1985, *An Atlas of Digital Spectra of Cool Stars*. Western Research Co., Tucson
- Tutukov A.V., 1978, A&A, 70, 57
- Ukita N., Goldsmith P.F., 1984, A&A, 138, 194
- van Belle G.T., Creech-Eakman M.J., Hart A., 2009, MNRAS, 394, 1925
- van Buren D., McCray R., 1988, ApJ, 329, L93
- van der Hucht K.A., 2001, *New Astron. Rev.*, 45, 135
- van Loon J.Th., Cioni M.-R.L., Zijlstra A.A., Loup C., 2005, A&A, 438, 273
- van Marle A.J., Meliani Z., Keppens R., Decin L., 2011, ApJ, 734, L26
- Vassilev V. et al., 2008, A&A, 490, 1157
- Verheyen L., Messineo M., Menten K.M., 2012, A&A, 541, A36
- Verhoelst T., Van der Zypen N., Hony S., Decin L., Cami J., Eriksson K., 2009, A&A, 498, 127
- Wareing C.J., Zijlstra A.A., O'Brien T.J., 2007a, ApJ, 660, L129
- Wareing C.J., Zijlstra A.A., O'Brien T.J., 2007b, MNRAS, 382, 1233
- Watson C.L., Henden A.A., Price A., 2006, in Warner B.D. et al., eds, *Society for Astronomical Sciences Annual Symposium Vol. 25, The International Variable Star Index (VSX)*. SAS, Rancho Cucamongo, CA, p. 47
- Weaver R., McCray R., Castor J., Shapiro P., Moore R., 1977, ApJ, 218, 377
- Wing R.F., 2009, in Luttermoser D.G., Smith B.J., Stencil R.E., eds., *The Biggest, Baddest, Coolest Stars*, ASP Conf. Ser. 412, 113
- Wright E.L. et al., 2010, AJ, 140, 1868
- Xu Y., Reid M.J., Zheng X.W., Menten K.M., 2006, Science, 311, 54
- Xu Y., Moscadelli L., Reid M.J., Menten K.M., Zhang B., Zheng X.W., Brunthaler A., 2011, ApJ, 733, 25
- Yang M., Jiang B.W., 2012, ApJ, 754, 35
- Zacharias N., Finch C.T., Girard T.M., Henden A., Bartlett J.L., Monet D.G., Zacharias M.I., 2013, AJ, 145, 44
- Zhu Z.X., Friedjung M., Zhao G., Hang H.R., Huang C.C., 1999, A&AS, 140, 69